Extended Abstracts of the 2002 International Conference on Solid State Devices and Materials, Nagoya, 2002, pp. 16–17

A-1-5

Multi-Subband Effects on the Performance Limit of Nanoscale MOSFETs

Kenji Natori, Tomo Shimizu and Tsuyoshi Ikenobe

Institute of Applied Physics, University of Tsukuba
Tsukuba, Ibaraki 305-8573, Japan
Phone: +81-298-53-5311, Fax: +81-298-53-5205 E-mail: natori@hermes.esys.tsukuba.ac.jp

1. Introduction

Recently, ultra-small MOSFETs of less than a few tens of nanometer size are ardently investigated [1] in request of the semiconductor roadmap. The performance limit of these nanoscale devices are known to be estimated by the ballistic MOSFET characteristics [2][3][4]. However, the estimation usually suggests a real MOSFET performance is far lower than the ideal value [3][5][6]. This paper shows that the multi-subband effect substantially revises the simple one-subband estimation and limits the ideal high performance even at room temperature. An improved value of the uppermost performance drawing nearer to the real ultra-small device value is also reported.

Conventional sub-micrometer MOSFETs were well described by the transport model using the carrier mobility, in which the carrier mean free path is required to be far smaller than the device size. In recent nanoscale MOSFETs, however, the device size is approaching to the mean free path and carriers suffer only a small number of scatterings in the course from the source to the drain. These "quasi-ballistic" MOSFETs are better analyzed by starting from the ballistic MOSFET without any scattering in the channel, and then introducing limited number of scattering events, as is illustrated in Fig. 1.

2. One-Subband versus Multi-Subband

Specifically, the ballistic MOSFET characteristics predict the uppermost high-performance of nanoscale MOSFETs, and the I-V characteristics of the n-channel ballistic MOS on Si (100) surface are expressed as in Figs. 2 and 3 [2]. The Multi-Subband Model (MSM) considers the many subband structure (actually 4 subbands in the following calculation) in n-Si 6 valleys correctly. The one-subband approximation considering the lowest subband is justified when most electrons resort to the lowest subband as is approximately satisfied in ultra-small MOSFETs. It is tractable because it allows a compact drain current expression in terms of terminal voltages. The higher subband contribution is effectively considered by modifying the parameter M_v, the number of lowest valleys (Effective One-Subband Approximation (EOSA)).

The saturation drain current of a ballistic MOSFET is represented by the current at the beginning of channel and is generally expressed as $I=W|Q|v_{inj}$ [2], where W is the channel width, $|Q|=C_{eff}(V_G-V_T)$ is the channel charge density at the source edge, and v_{inj} (injection velocity) is the velocity with which carriers are injected from the source electrode to the channel. The v_{inj} is a function of $|Q|$, and EOSA provides its value of $1.2\sim2\times10^7$cm/s, which predicts the MOS uppermost current distribute up to 3mA/μm in strong inversion. However, even a 15nm experimental MOSFET provides only 0.615 mA/μm [1], for example.

3. Results

The injection velocity and the drain current for both EOSA and MSM are evaluated and compared to each other. Subband levels for acceptor concentration of 10^{18}cm^{-3}, which value or even higher concentration is required in nanoscale MOSFETs, are computed in Hartree Approximation solving the Schrodinger equation and the Poisson equation self-consistently. The lowest 4 energy levels of E_0, E_0', E_1 and E_2, which are plotted in Fig. 4 as a function of $|Q|$, are considered in the analysis. The injection velocity v_{ijn} and the drain current I are computed by use of the formulae in Figs. 2 and 3 and the result is plotted in Figs. 5 and 6. v_{inj} in weak inversion is almost constant around 1.2×10^7cm/s, which is the thermal velocity of non-degenerate electron gas, $(2k_BT/\pi m_x)^{1/2}$. It increases as $|Q|$ increases in strong inversion due to the carrier degeneracy. But the value exceeding 2.0×10^7cm/s in EOSA is suppressed to less than 1.6×10^7cm/s by the multi-subband effect. The fact that v_{inj} is confined within a narrow region between 1.2×10^7cm/s and 1.6×10^7cm/s means the carrier degeneracy effect is limited at the room temperature. The drain current in Fig. 6 shows the overall behavior is analogous to that of v_{inj}, curve, but notice that the multi-subband effect reduces its magnitude to around 80% of the EOSA value for large $|Q|$. Fig. 7 shows the fraction of the lowest subband carriers to the total channel carrier, which is around 80% and goes lower for large $|Q|$. Table I compares performance of nanoscale MOSFETs reported recently. The ballisticity r is so defined that r=(experimental MOS I_{sat})/(ballistic MOS I_{sat}). Notice that EOSA significantly underestimates the value. Although estimation of source/drain resistance includes ambiguity, the case r=0.69 asserts that more than 80% of injected carriers escape back-scattering to source and reach drain. The newer and smaller MOSFETs tend to have lower ballisticity.

4. Conclusions

Compared to the simple EOSA method, the more rigorous MSM estimation provides a 20% smaller value for the uppermost performance of nanoscale MOSFET. The result indicates the recent nanoscale MOSFET report may include devices operating at close to the ideal ballistic limit.

References

[1] B. Yu et al., IEDM Tech. Digest, pp. 937 (2001)

[2] K. Natori, J. Appl. Phys. **76**, 4879 (1994)

[3] K. Natori, IEICE Trans. Electron. **E84-C**, 1029 (2001)

[4] F. Assad et al., IEEE Trans. Electron Devices **47**, 232 (2000)

[5] F. Assad et al., IEDM Tech. Digest, pp. 547 (1999)

[6] A. Lchtefeld, IEEE Electron Device Lett. **22**, 95 (2001)

[7] H.Wakabayashi et al., IEDM Tech. Digest, pp. 49 (2000)

[8] G. Timp et al., IEDM Tech. Digest, pp. 55 (1999)

[9] R. Chau et al., IEDM Tech. Digest, pp. 45 (2000)

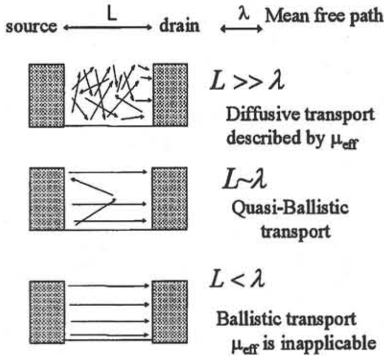

Fig. 1. Carrier transport in MOSFET

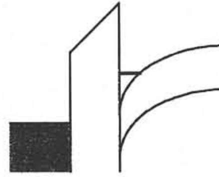

A compact current expression

$$I_D = \frac{\sqrt{2m_t}\, q(kT)^{3/2} M_v}{\pi^2 \hbar^2}\left[F_{1/2}(u) - F_{1/2}(u - v_d)\right],$$

$$u = \ln\left[\sqrt{(1+e^{v_d})^2 + 4e^{v_d}(e^{\rho} - 1)} - (1+e^{v_d})\right] - \ln 2,$$

$$v_d = \frac{qV_D}{kT}, \qquad \rho = \frac{2\pi\hbar^2 C(V_G - V_t)}{qkTm_t M_v}.$$

Fig. 2. Effective One-Subband Approximation (EOSA)

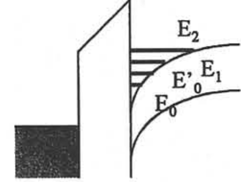

$$I_D = \frac{\sqrt{2}\, q(kT)^{3/2}}{\pi^2 \hbar^2} \sum_{valley} \sum_{n} \sqrt{m_y}\left[F_{1/2}\left(\frac{\phi_{FS} - E_n}{kT}\right) - F_{1/2}\left(\frac{\phi_{FS} - E_n - qV_D}{kT}\right)\right]$$

$$|Q| = C(V_G - V_t) = \frac{qkT}{2\pi\hbar^2} \sum_{valley} \sum_{n} \sqrt{m_x m_y} \times \ln\left\{\left[1 + \exp\left(\frac{\phi_{FS} - E_n}{kT}\right)\right]\left[1 + \exp\left(\frac{\phi_{FS} - E_n - qV_D}{kT}\right)\right]\right\}$$

Fig. 3. Multi-Subband Model (MSM)

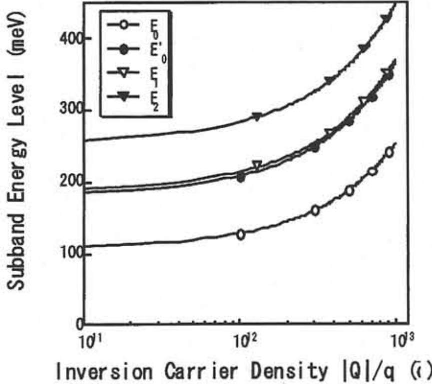

Fig. 4. Subband energy level as a function of inversion carrier density

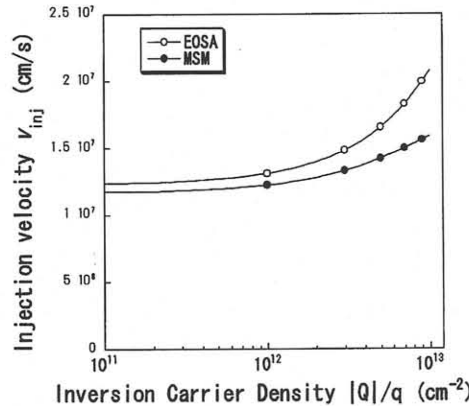

Fig. 5. Injection velocity as a function of inversion carrier density

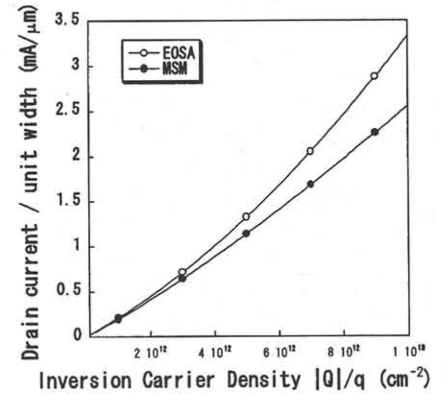

Fig. 6. Saturation current per unit width as a function of inversion carrier density

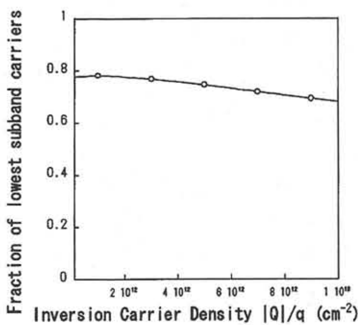

Fig. 7. Fraction of lowest subband carriers as a function of inversion carrier density

Table. I. Comparison of recent nanoscale MOSFET ballisticity. See Ref. [1][7][8][9].

Author	Wakabayashi	Timp	Cau	Yu
Company	NEC	Bell Lab	Intel	AMD
L(nm)	24	40	30	15
Conference	IEDM2000	IEDM1999	IEDM2000	IEDM2001
I/W(mA/um)	0.796	1.3	0.514	0.615
Tox(EOT) (nm)	2.5	1.3	1.9uF/cm2	0.8
r (EOSA, R(S/D) ignore)	0.31	0.43	0.29	0.16
r (MSM, R(S/D) ignore)	0.39	0.55	0.35	0.22
r (MSM, R(S/D) consider)	0.45	0.69	0.42	0.24